Magnetic correlations and pairing in the 1/5-depleted square lattice Hubbard model

Ehsan Khatami, Rajiv R. P. Singh, Warren E. Pickett, and Richard T. Scalettar

Department of Physics, University of California, Davis, CA 95616, USA

We study the single orbital Hubbard model on the 1/5-depleted square-lattice geometry, which arises in CaV_4O_9 and ordered-vacancy iron selenides. We find a rich phase diagram that includes a plaquette singlet phase, a dimer singlet phase, a Néel and a block-spin antiferromagnetic phase, and stripe phases. Quantum Monte Carlo simulations show that the dominant pairing correlations at half filling change character from d-wave in the plaquette phase to extended s-wave upon transition to the Néel phase. These findings have intriguing connections to iron-based superconductors, and suggest that tuning the doping in depleted geometries can capture physics related to multiple orbitals.

The interplay of magnetic order and pairing correlations has been a central topic in strongly correlated materials, and, in particular, in copper-based [1] and more recently iron-based [2] high-temperature superconductors. That pairing arises in intimate proximity to magnetism is initially somewhat surprising, since long-range magnetic order usually leads to an insulating Mott or Slater gap, which precludes superconductivity. Much study of these materials has been devoted to understanding how doping, and the presence of multiple bands, modify the magnetism [3–5] and allow pairing and short-range spin order to complement each other [6–16].

One geometry which has been a recurring structure in real materials, and which permits tuning of the degree of magnetic order, is the periodically 1/5-depleted square lattice, consisting of coupled plaquette unit-cells. It was first discovered in the study of spin-gap calcium vanadate material CaV_4O_9 [17]. More recently, the same structure arises in ordered vacancy iron selenide family of materials [18, 19]. One of the main reasons for the extensive interest in the calcium vanadates was to understand the potential connection between spin-gap behavior and superconductivity. However, these are strongly insulating materials and attempts to dope them and obtain a superconducting state were not successful. In contrast, the iron selenides clearly show magnetic, insulating, metallic and superconducting phases [20]. The multi-band character of the latter allows much greater material flexibility. One particularly interesting open issue in the iron-based superconductors is the possibility of changing superconducting pairing symmetry between various s-wave and d-wave channels [14–16, 21, 22].

The Heisenberg model on the 1/5-depleted square lattice has been extensively studied using a variety of numerical and analytical techniques [23–26]. Its ground state phase diagram consists of two spin-gap phases adiabatically related to decoupled plaquettes and decoupled dimers respectively, with an intervening Néel phase. Both gapped phases are separated from the Néel phase by a second order quantum critical point in the universality class of the 3d classical Heisenberg model.

The dominant exchange constants in CaV_4O_9 turned out to be second-neighbor interactions [27], which can be mapped back into an equivalent square lattice of larger plaquettes, while the search for the simplest model for the iron chalcogenide family of materials remains ongoing [28].

Here, we study a single-orbital Hubbard Hamiltonian on the 1/5-depleted square lattice. Using the determinant quantum Monte Carlo (DQMC) method [29, 30], which has no 'minus-sign problem' [31] at half-filling on this lattice, we find that the dimerized phase of the large Hubbard U limit (Heisenberg model) connects smoothly to a band insulator as U goes to zero. However, as U decreases, the Néel phase extends farther and farther into the region where intra-plaquette hopping is dominant. The plaquette phase, at large U, is always separated from the metallic phase, obtained at $U = 0$, by an intervening Néel phase.

In the limit where the inter-plaquette hopping t' is much smaller than the intra-plaquette hopping t, our model is a variant of the weakly coupled plaquette model studied by Tsai and Kivelson [32]. This Hamiltonian can be rigorously shown to have pair-binding and a superconducting phase at infinitesimal doping away from half-filling for $U \lesssim 4.6t$, a property which remains true for our model as well. Our QMC simulations extend the result away from small t' and demonstrate that singlet pairing is predominantly in the d-wave channel in the plaquette phase and becomes particularly large as U exceeds one half of the noninteracting bandwidth. We also find that, surprisingly, as soon as one approaches the phase transition to the Néel order, the dominant pairing changes from d-wave to extended s-wave. To our knowledge, there has been no previous unbiased demonstration of interchange of superconducting pairing symmetry with change in the magnetic properties, emphasizing the close interplay of magnetic and superconducting correlations in these systems.

Indeed, this observation has possible connections to the iron selenide materials whose magnetic phases include ubiquitous stripe phases and a 2×2 block-spin antiferromagnet [18–20, 33, 34]. In the latter,

spins within a plaquette align, and these block-spins then order in an antiferromagnetic pattern. Using the random phase approximation (RPA), we have explored a number of different magnetic instabilities in the 1/5-depleted geometry. At half-filling, the dominant order in our nearest-neighbor (NN) model is the usual Néel phase. However, away from half filling, both the stripe phase as well as the 2×2 block-spin antiferromagnet are found to be the leading instabilities over different doping ranges, remarkably, showing that such phases can arise in models without requiring any frustration or multi-orbital character.

The Hubbard Hamiltonian considered here is,

$$\hat{H} = - \sum_{ij\sigma} t_{ij} c_{i\sigma}^{\dagger} c_{j\sigma} - \mu \sum_{i\sigma} n_{i\sigma}$$
$$+ U \sum_i (n_{i\uparrow} - \frac{1}{2})(n_{i\downarrow} - \frac{1}{2}). \quad (1)$$

Here, $c_{i\sigma}$ ($c_{i\sigma}^{\dagger}$) annihilates (creates) a fermion with spin σ on site i, $n_{i\sigma} = c_{i\sigma}^{\dagger} c_{i\sigma}$ is the number operator, U is the onsite repulsive Coulomb interaction, and t_{ij} is the hopping matrix element between sites i and j. We allow for NN hopping only and consider two different values: $t_{ij} = t$ if i and j are nearest neighbors within a plaquette, $t_{ij} = t'$ if i and j are nearest neighbors on a bond that connects two distinct plaquettes, and $t_{ij} = 0$ otherwise. At $U = 0$, there are four bands with dispersion $\epsilon_\alpha(k)$ given by the roots of, $(\epsilon_\alpha^2(k) - t'^2)^2 - 4t^2(\epsilon_\alpha(k) + t'\cos k_x)(\epsilon_\alpha(k) + t'\cos k_y) = 0$. As we vary the ratio t'/t, the noninteracting bandwidth $w = 4t + 2t'$ is kept fixed at 6, setting the unit of energy to $w/6$ throughout this paper.

The richness of the band structure has prompted a recent mean-field study of the model at quarter filling, where there is on average one half particle per site [35]. When $t' = t$, the Fermi energy at this filling coincides with a Dirac cone structure at the zone center and a flat band in its proximity. Yasufumi *et al.* [35] identify three different phases: a paramagnetic insulator, a paramagnetic metal, and an antiferromagnet, for which phase transitions could be described by an effective SU(3) theory. The Mott transition in the dimer region has also been recently studied within a cluster dynamical mean-field theory [36].

The phase diagram at half-filling in the plane of t'/t and $U/(1 + U)$ is given in Fig. 1. It establishes the dominant magnetic instability as antiferromagnetism. The range of t/t' for which the ground state is Néel ordered is shown as thick horizontal lines for three different values of U. At $U \ll 1$, the AF region extends from an infinitesimal t' all the way to $t'/t = 2$, beyond which the non-interacting system is a band insulator. The Néel phase in this regime is favored by AF nesting at the Fermi surface for $t' < 2t$, and the fact that the growing nested area compensates for the loss of isotropy
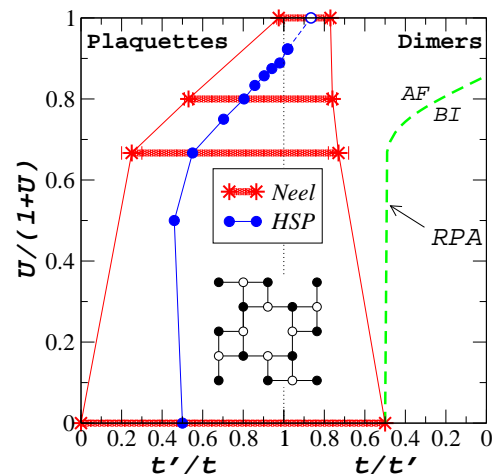

FIG. 1. Ground state phase diagram at half filling. The thick horizontal lines indicate the region with long-range Néel order. At $U = \infty$, the AF region is obtained from Ref. 25 (Heisenberg model study on the same geometry) by considering $t'/t = \sqrt{J'/J}$. Here, J and J' are the intra- and inter-plaquette spin exchange interactions. Blue circles track the high symmetry point (HSP) inside the AF region where the NN spin correlations are equal on all bonds (see Fig. 2). Similar results for the HSP are not available for the Heisenberg limit. So instead, the empty blue circle indicates the location of the maximum of the AF moment in that limit. The dashed line shows the AF/band insulator (BI) phase boundary as predicted by the RPA. The inset depicts the AF ordering of up (filled circles) and down (empty circles) spins.

in the system as $t' \to 0$. We obtain this range from the RPA, which is exact in that limit (the RPA estimate for the AF phase boundary at nonzero U is also shown by a dashed line in Fig. 1).

As we turn on the interaction, we find that for t and t' sufficiently close to each other, there is always a non-zero Néel order parameter in the thermodynamic limit. We locate the phase boundary by finite-size scaling of the DQMC AF structure factor, S_{AF} [30]. One can see that as U increases, the Néel ordered region shrinks, especially on the plaquette side, and moves to the Heisenberg limit ($U \to \infty$) range [25].

Also shown as filled circles in the phase diagram of Fig. 1 are the hopping ratios at which the intra- and inter-plaquette NN spin correlations are equal in magnitude. This line of 'high symmetry points' (HSPs) favors the plaquette side of the phase diagram until it veers toward the dimer side around $U = 3$, tracking the magnetically ordered region.

Figure 2(a) shows the absolute value of the difference of NN spin correlations on the two types of bonds at inverse temperature $\beta = 20$ as a function of hopping ratios. At the weakest coupling $U = 1$ the NN spin correlation on the intra-plaquette t bonds exceeds the inter-plaquette t' bonds up to $t'/t \sim 0.5$, at which point the relative
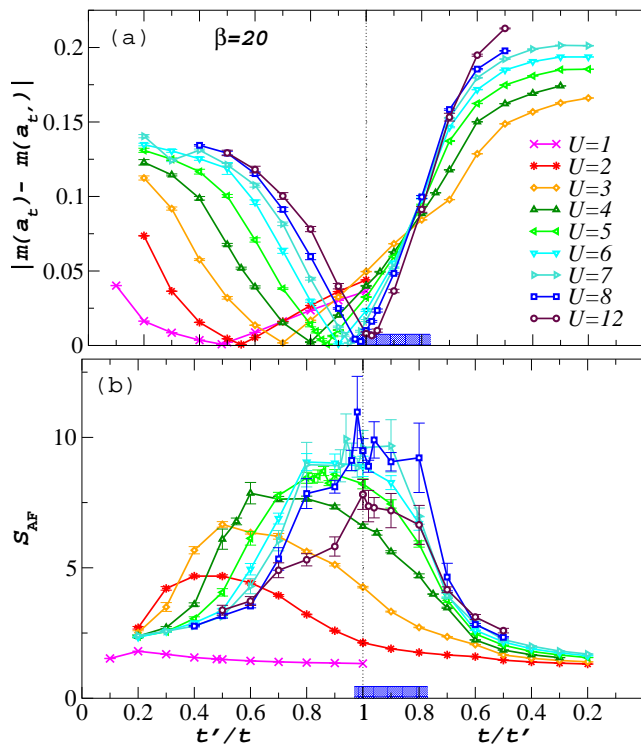
FIG. 2. (a) The absolute value of the difference in the NN spin correlations [30] on t and t' bonds at $\beta = 20$ from DQMC vs t'/t for several values of the interaction strength ('a' denotes the lattice constant between NNs). The shaded region on the horizontal axis is added to show the boundaries of the Néel phase in the $U \to \infty$ limit. The lattice is a 4×4 arrangement of 2×2 plaquettes ($N = 64$), except for $U = 1$ and 2 where the 8×8 arrangement ($N = 256$) is used. We have also simulated a 576-site lattice for the latter interactions and found no significant changes in the location of the HSP (b) The AF structure factor vs t'/t at $\beta = 20$ from DQMC. Except for $U = 1$, for which $N = 256$, the results are obtained for the $N = 64$ lattice.
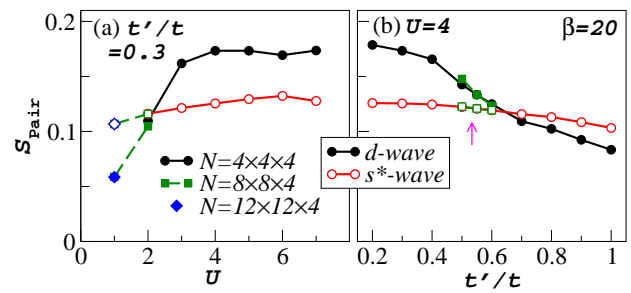

FIG. 3. (a) Pairing structure factor [30] at $\beta = 20$ and $t'/t = 0.3$ vs the interaction strength. For $U = 1$ and 2, two different system sizes are shown. (b) Pairing structure factor at $\beta = 20$ and $U = 4$ vs the ratio t'/t. Full (Empty) symbols are for the d-wave (extended s-wave) symmetry. The error bars are smaller than the symbols. The arrow indicates the location of the AF phase transition.

size is reversed [37]. However, at the strongest coupling studied, $U = 12$, the intra-plaquette spin correlation remains larger all the way to $t'/t \sim 1$. The finite-size dependence of these correlations is either negligible, or has been taken into account [30] (see caption of Fig. 2 for details). We note that all of the calculated NN spin correlations are antiferromagnetic, regardless of the value of t'/t or U.

The results in Fig. 2(b), show the low-temperature S_{AF} as a function of the hopping ratios for the same range of interaction strengths as in Fig. 2(a). Although these results are for a single (relatively large) lattice size, the evolution of the peak of S_{AF} clearly conveys the trend in the long-range order as U is increased towards the Heisenberg limit. These maxima shift steadily from the plaquette side at weak coupling to the dimer side at strong coupling.

An intriguing feature seen in this model is the change

in symmetry of low-temperature pairing correlations from d-wave in the plaquette phase to extended s-wave upon entering the Néel phase. This is demonstrated in Fig. 3, where we plot the uniform pairing structure factor [30] for the two symmetries vs the interaction strength at $t'/t = 0.3$, and vs the hopping ratio at $U = 4$, for which we know the location of the AF phase transitions. As shown in Fig. 3, finite-size effects at small U are not responsible for this difference. We have also verified that the values of the structure factor do not change by further lowering the temperature. At $U = 4$, the change in the pairing symmetry takes place inside the AF region just before the transition to the plaquette phase. For all the other interaction strengths, the location of this crossover appears to fall to the right (larger t' side) of the AF phase boundary. As the charge gap is nonzero in both the AF and the plaquette phase, we do not expect to find superconductivity at half filling. However, the strength of the pairing at half-filling should be indicative of the nature of superconductivity upon doping. The d-wave pairing in the weakly-coupled plaquette phase agrees with the general arguments of Scalapino and Trugman [38] and of Tsai and Kivelson [32]. The dominance of extended s-wave pairing near the phase transition is a surprising result and points to the close interplay between magnetism and superconductivity in these systems.

We now turn to the case away from half filling, where we use the RPA instead of the DQMC, as low-temperature results are not available for the latter. Figure 4 provides the full evolution of the critical interaction strength U_c for six different magnetic orderings as a function of the electron density, ρ, in the uniform $t = t'$ case. Four of the magnetic phases are shown atop the main panel in Fig. 4. The other two are the regular $Q = (\pi, \pi)$ AF (shown in Fig. 1) and the simple $Q = (0, 0)$ ferromagnetic (FM) phases. Here, Q is
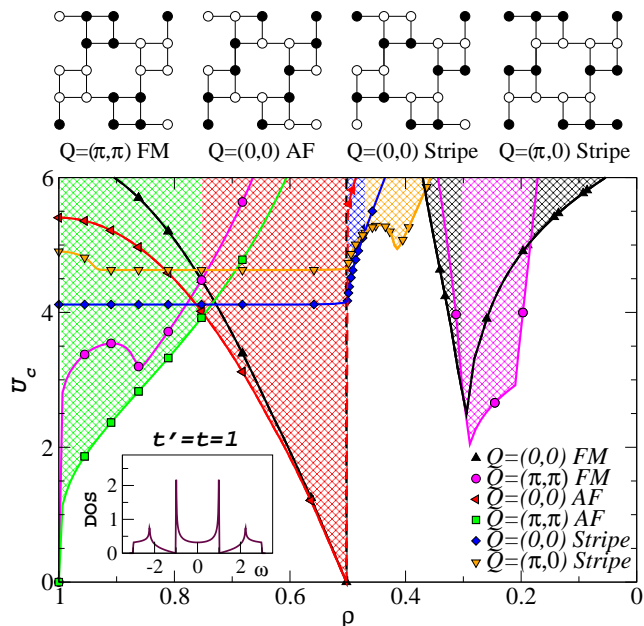
FIG. 4. (Top) Four of the magnetic orderings considered in this study. The up (down) spins are denoted by filled (empty) circles. Q indicates the phase between unit cells and the FM, AF, and Stripe denote the ordering of spins within each unit cell. (Bottom) The ground state RPA phase diagram of the model at $t' = t$ away from half filling. The inset shows the density of states (DOS).

the wave vector corresponding to the superlattice and the following letters describe the order within a plaquette. The $Q = (\pi, \pi)$ AF dominates near half-filling and up to $\rho \sim 0.75$. At that point, the $Q = (0, 0)$ AF has the largest susceptibility and hence, the smallest U_c, even though for densities close to, but higher than $\rho = 0.5$ (quarter filling), it is degenerate with the $Q = (0, 0)$ FM phase. Exactly at quarter filling, we find that the $Q = (0, 0)$ Stripe, and not the $Q = (0, 0)$ AF, as predicted by a previous mean-field calculation [35], is the dominant order. However, at a slightly smaller ρ, this order is replaced by the $Q = (\pi, 0)$ Stripe order. Interestingly, at $\rho \sim 1/3$, the block AF phase, observed in ordered-vacancy iron selenide materials, has the lowest U_c. This order shows up at even lower energies in the anisotropic case of $t' < t$. Thus, in many ways, the single-orbital model at different dopings captures the richness of the magnetic phases observed in the iron pnictide and chalcogenide family of materials.

Quantum Monte Carlo methods allow for an exact treatment of the combined effects of correlation and band structure on lattices of finite spatial size, or equivalently, with finite resolution in momentum space. Previous DQMC studies of the effect of multiple bands and different inter-site hoppings on magnetic order have mostly been confined to layered geometries in which two spatially extended regions each with a unique

hopping are coupled [39–41]. Here, in contrast, we have presented results for a hopping pattern in which two different t_{ij} are mixed locally, and found that, tuning their ratio leads to multiple quantum phase transitions and rich phase diagrams. We have also studied the superconducting properties of our model at half filling within the DQMC. Remarkably, the dominant pairing symmetry changes character from d-wave in the plaquette phase to an extended s-wave in the Néel phase, revealing an interesting interplay between magnetic and superconducting correlations. Although our system is insulating at half filling, the dominant pairing at half-filling should be an indicator of the nature of superconductivity upon doping. Moreover, the behavior of both the magnetic and superconducting correlations in our single-orbital model offer surprising connections to iron-based superconductors, which are multi-orbital systems, implying that they can be mapped to effective one-orbital models but with varying doping values.

[1] E. Dagotto, Rev. Mod. Phys. **66**, 763 (1994).
[2] G. R. Stewart, Rev. Mod. Phys. **83**, 1589 (2011).
[3] M. J. Han, Q. Yin, W. E. Pickett, and S. Y. Savrasov, Phys. Rev. Lett. **102**, 107003 (2009).
[4] I. I. Mazin and M. D. Johannes, Nat Phys **5**, 141 (2009).
[5] P. Dai, J. Hu, and E. Dagotto, Nat Phys **8**, 709 (2012).
[6] C. de la Cruz, Q. Huang, J. W. Lynn, J. Li, W. R. II, J. L. Zarestky, H. A. Mook, G. F. Chen, J. L. Luo, N. L. Wang, et al., Nature **453**, 899 (2008).
[7] C. Xu, M. Müller, and S. Sachdev, Phys. Rev. B **78**, 020501 (2008).
[8] A. V. Chubukov, D. V. Efremov, and I. Eremin, Phys. Rev. B **78**, 134512 (2008).
[9] Q. Si and E. Abrahams, Phys. Rev. Lett. **101**, 076401 (2008).
[10] G. S. Uhrig, M. Holt, J. Oitmaa, O. P. Sushkov, and R. R. P. Singh, Phys. Rev. B **79**, 092416 (2009).
[11] I. I. Mazin, D. J. Singh, M. D. Johannes, and M. H. Du, Phys. Rev. Lett. **101**, 057003 (2008).
[12] R. M. Fernandes, D. K. Pratt, W. Tian, J. Zarestky, A. Kreyssig, S. Nandi, M. G. Kim, A. Thaler, N. Ni, P. C. Canfield, et al., Phys. Rev. B **81**, 140501 (2010).
[13] R. M. Fernandes and J. Schmalian, Phys. Rev. B **82**, 014521 (2010).
[14] K. Okazaki, Y. Ota, Y. Kotani, W. Malaeb, Y. Ishida, T. Shimojima, T. Kiss, S. Watanabe, C.-T. Chen, K. Kihou, et al., Science **337**, 1314 (2012).
[15] Q. Q. Ge, Z. R. Ye, M. Xu, Y. Zhang, J. Jiang, B. P. Xie, Y. Song, C. L. Zhang, P. Dai, and D. L. Feng, Phys. Rev. X **3**, 011020 (2013).
[16] N. Xu, P. Richard, X. Shi, A. van Roekeghem, T. Qian, E. Razzoli, E. Rienks, G.-F. Chen, E. Ieki, K. Nakayama,

et al., Phys. Rev. B **88**, 220508 (2013).

[17] S. Taniguchi, T. Nishikawa, Y. Yasui, Yukio Kobayashi, J. Takeda, S.-I. Shamoto, and M. Sato, J. Phys. Soc. Jpn. **64**, 2758 (1995).

[18] B. Wei, H. Qing-Zhen, C. Gen-Fu, M. A. Green, W. Du-Ming, H. Jun-Bao, and Q. Yi-Ming, Chinese Physics Letters **28**, 086104 (2011).

[19] F. Ye, S. Chi, W. Bao, X. F. Wang, J. J. Ying, X. H. Chen, H. D. Wang, C. H. Dong, and M. Fang, Phys. Rev. Lett. **107**, 137003 (2011).

[20] E. Dagotto, Rev. Mod. Phys. **85**, 849 (2013).

[21] R. Thomale, C. Platt, W. Hanke, J. Hu, and B. A. Bernevig, Phys. Rev. Lett. **107**, 117001 (2011).

[22] S. Maiti, M. M. Korshunov, T. A. Maier, P. J. Hirschfeld, and A. V. Chubukov, Phys. Rev. Lett. **107**, 147002 (2011).

[23] N. Katoh and M. Imada, J. Phys. Soc. Jpn. **64**, 4105 (1995).

[24] K. Ueda and H. Kontani, Phys. Rev. Lett. **76**, 1932 (1996).

[25] M. Troyer, H. Kontani, and K. Ueda, Phys. Rev. Lett. **76**, 3822 (1996).

[26] M. P. Gelfand, Z. Weihong, R. R. P. Singh, J. Oitmaa, and C. J. Hamer, Phys. Rev. Lett. **77**, 2794 (1996).

[27] W. E. Pickett, Phys. Rev. Lett. **79**, 1746 (1997).

[28] J. K. Glasbrenner, J. P. Velev, and I. I. Mazin, Phys. Rev. B **89**, 064509 (2014).

[29] R. Blankenbecler, D. J. Scalapino, and R. L. Sugar, Phys. Rev. D **24**, 2278 (1981).

[30] See Supplementary Materials for a discussion of the DQMC method, finite-size scaling of the AF structure factors, and a brief discussion of the RPA.

[31] E. Y. Loh, J. E. Gubernatis, R. T. Scalettar, S. R. White, D. J. Scalapino, and R. L. Sugar, Phys. Rev. B **41**, 9301 (1990).

[32] W.-F. Tsai and S. A. Kivelson, Phys. Rev. B **73**, 214510 (2006).

[33] Q. Luo, A. Nicholson, J. Riera, D.-X. Yao, A. Moreo, and E. Dagotto, Phys. Rev. B **84**, 140506 (2011).

[34] H. Li and Y. Liu, EPL (Europhysics Letters) **98**, 47006 (2012).

[35] Y. Yamashita, M. Tomura, Y. Yanagi, and K. Ueda, Phys. Rev. B **88**, 195104 (2013).

[36] Y. Yanagi and K. Ueda, arXiv:1403.1743 (unpublished) (2014).

[37] For $U = 0$, exact results for clusters as large as $N = 1024$ and at lower temperatures lead to $t'/t = 0.5$ as the location of the HSP.

[38] D. J. Scalapino and S. A. Trugman, Philosophical Magazine Part B **74**, 607 (1996).

[39] R. T. Scalettar, J. W. Cannon, D. J. Scalapino, and R. L. Sugar, Phys. Rev. B **50**, 13419 (1994).

[40] A. Euverte, F. Hebert, S. Chiesa, R. Scalettar, and G. Batrouni, Phys. Rev. Lett. **108**, 246401 (2012).

[41] A. Euverte, S. Chiesa, R. Scalettar, and G. Batrouni, Phys. Rev. B **88**, 235123 (2013).

[42] D. A. Huse, Phys. Rev. B **37**, 2380 (1988).

Supplementary Materials for EAPS:
Magnetic correlations and pairing in the 1/5-depleted square lattice Hubbard model

Ehsan Khatami, Rajiv R.P. Singh, Warren E. Pickett, Richard T. Scalettar

Department of Physics, University of California, Davis, California 95616, USA

METHOD

In the determinantal quantum Monte Carlo (DQMC), the exponential $\exp(-\beta\hat{H})$ in the partition function is written as a product of incremental imaginary time propagators $\exp(-\Delta\tau\hat{H})$ where $\beta = L\Delta\tau$ is the inverse temperature. The Trotter approximation $\exp(-\Delta\tau\hat{H}) \approx \exp(-\Delta\tau\hat{K})\exp(-\Delta\tau\hat{V})$ is used to isolate the exponential of the on-site interaction $\hat{V}$ from the kinetic energy and chemical potential terms $\hat{K}$.

A (discrete) Hubbard-Stratonovich (HS) variable $s_{i\tau}$ is introduced at each spatial site i and imaginary time slice τ to decouple the interaction term,

$$e^{-U\Delta\tau(n_{i\uparrow}-\frac{1}{2})(n_{i\downarrow}-\frac{1}{2})} =$$
$$\frac{1}{2}e^{-U\Delta\tau/4}\sum_{s_{i\tau}=\pm 1}e^{\lambda s_{i\tau}(n_{i\uparrow}-n_{i\downarrow})} \quad (2)$$

where $\cosh\lambda = e^{U\Delta\tau/2}$. The quartic term in fermion creation and destruction operators is thereby replaced by quadratic terms coupled to the HS field $\{s_{i\tau}\}$. The fermion degrees of freedom can be traced out analytically, leaving a sum over $\{s_{i\tau}\}$ to be performed stochastically (using Monte Carlo).

The result of tracing over the fermion degrees of freedom is a product of two determinants, one for each spin species. In general, this product can go negative, precluding its use as a Monte Carlo weight. This is known as 'the sign problem' [31], and results in a limit on the temperatures accessible to the simulation. In special cases, such as at half filling ($\mu = 0$) and with a bipartite lattice, the signs of the two determinants are always equal and it is possible to make β very large. However, at generic fillings, the constraint is typically $\beta t \lesssim 4$ (although the precise value depends on the average density ρ, the interaction strength U, and the lattice size). For this reason, we focus on half filling (which is, anyway, also the density for which the mapping to the Heisenberg model is valid), and use the analytic RPA treatment to discuss doped lattices. In the work reported here, we use $\Delta\tau = 1/2U$, except for $U = 1$ where $\Delta\tau = 1/4$, to keep the associated Trotter errors smaller than statistical ones from the Monte Carlo sampling of the HS field.

Magnetic properties of the model are determined by the real space spin-spin correlation functions

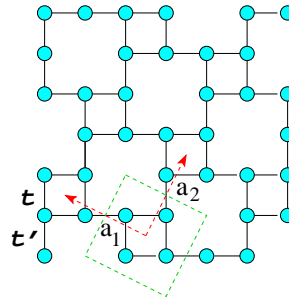$$m^{xx}(\mathbf{r}) = \langle S^-(i+\mathbf{r})S^+(i)\rangle$$

FIG. 5. The geometry of the 1/5-depleted lattice. 2×2 plaquettes have inter-site hopping t. Different plaquettes are linked by hopping t'. The two primitive vectors are shown by red arrows and the unit cell is shown by the tilted square.

$$m^{zz}(\mathbf{r}) = \langle S^z(i+\mathbf{r})S^z(i)\rangle, \quad (3)$$

where

$$S^+(i) = c_{i\downarrow}c_{i\uparrow}^\dagger$$
$$S^-(i) = c_{i\uparrow}c_{i\downarrow}^\dagger$$
$$S^z(i) = \frac{1}{2}(n_{i\uparrow} - n_{i\downarrow}), \quad (4)$$

their average along an arbitrary direction

$$m(\mathbf{r}) = \frac{1}{3}[2m^{xx}(\mathbf{r}) + m^{zz}(\mathbf{r})], \quad (5)$$

and its Fourier transform, the magnetic structure factor,

$$S(\mathbf{q}) = \sum_{\mathbf{r}}e^{i\mathbf{q}\cdot\mathbf{r}}m(\mathbf{r}). \quad (6)$$

When long-range order with wavevector $\mathbf{q}$ is present in $m(\mathbf{r})$, the spatial sum in Eq. 6 at the corresponding $\mathbf{q}$ diverges in the thermodynamic limit, since the sum over $\mathbf{r}$ grows linearly with N. Spin wave theory [42] predicts that the finite-size correction is linear in the inverse lattice size L, so that $S(\mathbf{q})/N = A + B/L$, where A is proportional to the square of the magnetic order parameter. In the disordered phase, the sum cuts off and $S(\mathbf{q})/N$ is proportional to $1/N = 1/L^2$. Note that here, $\mathbf{q}$ denotes both the phase between sites of a unit cell, and $\mathbf{Q}$, the wavevector describing the phase between unit cells.

We consider six possibilities for the spatial structure of the magnetic order on the lattice of Fig. 5. Four of them are illustrated in Fig. 4 of the main text. The other two are the regular antiferromagnetic (AF) order, illustrated
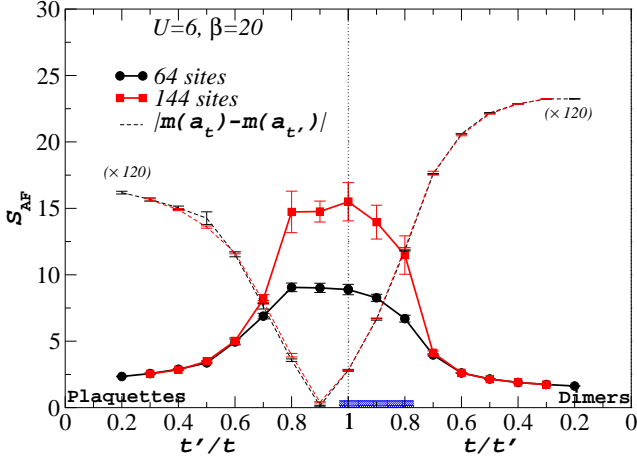
FIG. 6. The AF structure factor S_{AF} for $U = 6$ at $\beta = 20$ vs t'/t for two different system sizes. The difference in the NN spin correlations for the same parameters is also shown for the two sizes. The blue (shaded) region indicates the range of t'/t for which the infinite-U limit exhibits long-range AF order.

in Fig. 1 of the main text, where the sign of the spin alternates between nearest-neighbor (NN) sites and the FM in which all spins are pointing to the same direction.

The magnetic susceptibility can also be evaluated in DQMC by considering spin correlation functions in real time and separated by imaginary time τ, e.g.,

$$m^{xx}(\mathbf{r}, \tau) = \langle S^-(i + \mathbf{r}, \tau) S^+(i, 0) \rangle$$
$$S^+(i, \tau) = e^{\tau \hat{H}} c_{i\downarrow} c_{i\uparrow}^\dagger e^{-\tau \hat{H}}, \tag{7}$$

and integrating over τ,

$$\chi(\mathbf{q}) = \int_0^\beta d\tau \sum_{\mathbf{r}} e^{i\mathbf{q}\cdot\mathbf{r}} m(\mathbf{r}, \tau). \tag{8}$$

However, for the determination of the phase diagram, the equal time structure factor is sufficient.

Similarly, one can define the equal-time pairing structure factor as

$$S_{\mathrm{Pair}}(\mathbf{q}) = \sum_{\mathbf{r}} e^{i\mathbf{q}\cdot\mathbf{r}} C(\mathbf{r}), \tag{9}$$

where

$$C(\mathbf{r}) = \langle \Delta_\alpha^\dagger(i + \mathbf{r}) \Delta_\alpha(i) + \Delta_\alpha(i + \mathbf{r}) \Delta_\alpha^\dagger(i) \rangle \tag{10}$$

is the pair-pair correlation function. Here, the pairing operator for the symmetry α is defined as

$$\Delta_\alpha(i) = \sum_{j \text{ NN of } i} f_\alpha(j)(c_{i\uparrow}c_{j\downarrow} - c_{i\downarrow}c_{j\uparrow}), \tag{11}$$

In case of the extended s-wave symmetry, $f_\alpha(j)$ is +1 for all of the three NN of i, and for the d-wave symmetry, $f_\alpha(j)$ is +1 if j is a NN of i along the x axis and −1 is along the y axis. We consider $S_{\mathrm{Pair}}(\mathbf{q} = 0)$ as the pairing structure factor, which is shown in Fig. 3 of the main text.
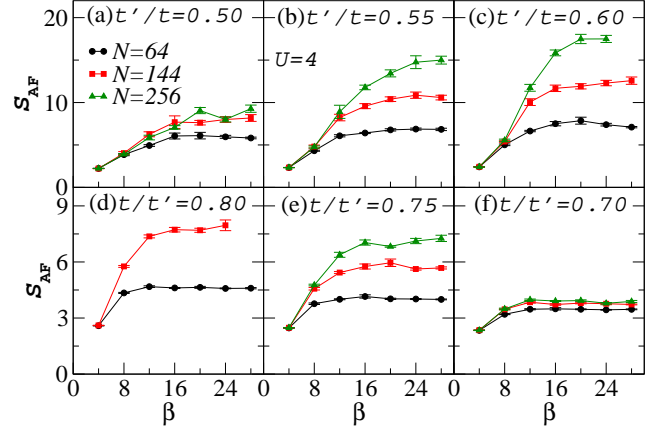

FIG. 7. The AF structure factor S_{AF} vs inverse temperature for several values of t'/t and three system sizes. For most cases, S_{AF} plateaus at or below $\beta = 20$.
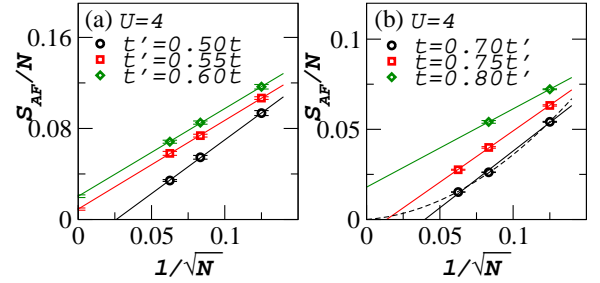

FIG. 8. Normalized AF structure factor vs the linear size of the system at $U = 4$ and for several ratios of t'/t. The extrapolated values in the thermodynamic limit are used to estimate the Néel phase boundary at this interaction strength. Solid lines are linear fits and the dashed line in (b) is a parabolic fit that passes through the origin.

ANTIFERROMAGNETIC PHASE TRANSITIONS

Figure 6 gives additional insight into the finite size scaling of the AF structure factors shown in Fig. 2(b) of the main text by exhibiting its behavior at $U = 6$ with changing the hopping ratio for two lattice sizes. For a range of values within the peak, S_{AF} is not only large, but also grows significantly with lattice size, giving rise to the nonzero $1/L \to 0$ extrapolations discussed below. We are also plotting in Fig. 6 the NN spin correlation difference for the two different system sizes, which supports our claim that the finite-size corrections for this quantity are generally negligible.

In order to make sure that $\beta = 20$ is a low enough temperature to describe the ground state properties of the lattice sizes we have considered, we show in Fig. 7 the dependence of S_{AF} at $U = 4$ on the inverse temperature across the two transition points to the Néel phase. For each of the ratios of t'/t, S_{AF} saturates to a lattice size dependent value. The mean values after saturation are used to perform the extrapolations in Figs. 8(a) and

8(b). In almost all cases, the AF structure factor plateaus at or below $\beta = 20$.

In the Néel phase, the normalized structure factor approaches a finite value in the thermodynamic limit as a function of the inverse linear size of the system. In the disordered phases, one expects S_{AF}/N to vanish as $1/N$. Consequently, after proper fitting of the data, the two end points of the Néel region at $U = 4$ are estimated from the extrapolations of S_{AF} to the thermodynamic limit for several values of the t'/t in their proximity as shown in Figs. 8(a) and 8(b).

RANDOM PHASE APPROXIMATION

In the RPA method, the non-interacting magnetic susceptibility is evaluated via,

$$\chi_0^{\alpha\beta}(\mathbf{q}) = -\frac{1}{N} \sum_{\mathbf{k}} \sum_{\eta\nu} \frac{f_\eta(\mathbf{k}) - f_\nu(\mathbf{k}+\mathbf{q})}{\epsilon_\eta(\mathbf{k}) - \epsilon_\nu(\mathbf{k}+\mathbf{q})} \times$$

$$\mathcal{S}_{\alpha\eta}^*(\mathbf{k})\mathcal{S}_{\alpha\nu}(\mathbf{k}+\mathbf{q})\mathcal{S}_{\beta\eta}(\mathbf{k})\mathcal{S}_{\beta\nu}^*(\mathbf{k}+\mathbf{q}) \quad (12)$$

where $\mathcal{S}_{\eta\nu}(\mathbf{k})$ are the similarity transformations which diagonalize the 4×4 matrix defining the band structure for each momentum $\mathbf{k}$. Since the full susceptibility, within the RPA, is given by $\chi = \chi_0/(1-U\chi_0)$, a magnetic phase transition to a state with ordering vector $\mathbf{q}$ occurs when $U\chi_0$ reaches unity (Stoner criteron) at $U = U_c$. The RPA is exact in the limit $U \to 0$, and is expected to be reasonably accurate at weak coupling. We carry out the calculation of χ_0 with lattice sizes up to $40,000^2$ and at various low temperatures to be able to obtain results in the thermodyanamic limit at $T = 0$.

For every parameter set, the dominant magnetic order is the one with the smallest U_c. However, there are other, subleading, ordering modes with larger values of U_c. These modes do not, however, replace the leading order when their respective Stoner criteria are met, i.e., the simplest version of the RPA is no longer valid after the system enters a broken symmetry state.